activity in the 25 years before large earthquakes in the San Francisco Bay area (*21, 22*). Unlike those examples the activity in southern California neither surrounded nor partly enclosed the rupture zone of the Landers earthquake itself. Instead, it mainly surrounds the southern SAF. Thus, the pattern probably was not precursory to the Landers event; that pattern plus the Landers sequence, may be part of a long-term precursor to a future great earthquake along the SAF. The high rate of moderate to large events is likely to continue. Activity for moderate-sized shocks decreased markedly in the Bay area after the 1906 earthquake and remained low for several decades, as seems to have been the case for decades after the great 1857 event in southern California (*21, 22*). These patterns can be attributed to a long period of regional stress increase without large to great shocks followed by a regional decrease in stress at or near the times of such events.

In the 8.5-year period before the Desert Hot Springs earthquake of 1948 (near kilometer 100 in Fig. 1) shocks of $4 < \mathbf{M} < 5.5$ occurred about 15 times more frequently within a radius of about 50 km of the hypocenter of that event than in similar other time intervals (*1, 22*). That burst of activity ended with the 1948 earthquake. The sizes of the shocks involved in that precursory sequence, and the area over which they occurred are much smaller than those for the pattern that has existed since about 1986. Sykes and Seeber (*1*) proposed that, given its structural complexity, it was unlikely that the major tectonic knot near SGP would rupture in a great earthquake without first undergoing major permanent deformation involving either rotations or translations of nearby crustal blocks. One of the two precursory scenarios that they suggested was that the sequence that preceded the 1948 shock may be a scaled-down version of the sequence that will lead to a great earthquake that ruptures either the SGP or Coachella Valley segments of the SAF. The occurrence of the Landers sequence, other activity since 1986, and the movement of the large crustal block to the north of SGP in that sequence bear strong resemblance to that scenario. It should be remembered, however, that the historic record is short enough that we do not have information on seismicity patterns preceding great earthquakes in this region.

It had been estimated (6) that the chance was about 60% that one or more great earthquakes would occur along the SAF in southern California from 1988 to 2018. We conclude that the increase in moderate to large earthquakes since 1986 and the changes in stress along the SAF associated with the Landers sequence indicate that the probability of a great shock is now higher than that estimated in 1988.

REFERENCES AND NOTES

1. L. R. Sykes and L. Seeber, *Geology* **13**, 835 (1985).
2. J. C. Matti, D. M. Morton, B. F. Cox, *U.S. Geol. Surv. Open-File Rep. 85-365* (1985).
3. C. R. Allen, *Geol. Soc. Am. Bull.* **68**, 315 (1957).
4. C. Nicholson, L. Seeber, P. Williams, L. R. Sykes, *J. Geophys. Res.* **91**, 4891 (1986).
5. K. Sieh, M. Stuiver, D. Brillinger, *ibid.* **94**, 603 (1989).
6. Working Group on California Earthquake Probabilities, *U.S. Geol. Surv. Open File Rep. 88-398* (1988).
7. L. Erickson, thesis, Stanford University (1986).
8. Earthquake hypocenters from the California Institute of Technology earthquake catalog in the San Bernadino Mountains–eastern Mojave Desert region show few earthquakes with depths greater than 12 km.
9. **M** is calculated using the formula $\mathbf{M} = 2/3 \log M_0 - 6.05$ (M_0 in Newton meters) modified from T. C. Hanks and H. Kanamori, *J. Geophys. Res.* **84**, 2348 (1979). Seismic moments, M_0, are from preliminary moment tensor solutions calculated by the Harvard group and reported in the "Preliminary Determination of Epicenters Catalog" (U.S. Geological Survey, Reston, VA); J. Mori, K. Hudnut, L. Jones, E. Hauksson, and K. Hutton [*Eos* 73, 417 (1992)] reported that more recent estimates of the M_0 for the Landers earthquake are smaller than the original estimate.
10. The amount of slip in each event was chosen to match its preliminary seismic moment, given the assumed rupture area and rigidity. These average displacements were used for the following earthquakes in the 1992 sequence: 0.4 m, 23 April, Joshua Tree; 7.7 m, 28 June, Landers; 0.7 m, 28 June, Big Bear. The computed stresses are not greatly changed if the rupture depths are increased and the overall displacement decreased.
11. P. A. Reasenberg and R. W. Simpson, *Science* **255**, 1687 (1992).
12. A. H. Lachenbruch and A. McGarr, *U.S. Geol. Surv. Prof. Pap.* **1515**, 261 (1990).
13. J. R. Rice, in *Fault Mechanics and Transport Properties of Rock: a Festchrift in Honor of W. F. Brace*, B. Evans and T.-F. Wong, Eds. (Academic Press, San Diego, CA, 1992), pp. 475–503.
14. C. H. Scholz, *The Mechanics of Earthquakes and Faulting* (Cambridge Univ. Press, Cambridge, 1990), p. 328.
15. D. H. Oppenheimer, R. A. Reasenberg, R. W. Simpson, *J. Geophys. Res.* **93**, 9007 (1988).
16. F. M. Chester, J. P. Evans, R. L. Beigel, *ibid.*, in press.
17. D. W. Simpson, W. S. Leith, C. H. Scholz, *Bull. Seismol. Soc. Am.* **78**, 2025 (1988).
18. J. H. Healy, W. W. Rubey, D. T. Griggs, C. B. Raleigh, *Science* **161**, 1301 (1968).
19. C. H. Scholz, C. Aviles, S. Wesnousky, *Bull. Seismol. Soc. Am.* **76**, 65 (1986).
20. G. King and J. Nábělek, *Science* **228**, 984 (1985).
21. W. L. Ellsworth, *U.S. Geol. Surv. Prof. Pap.* **1515**, 153 (1990).
22. L. R. Sykes and S. C. Jaumé, *Nature* **348**, 595 (1990).
23. C. W. Jennings, fault map of California, Sacramento, California Division of Mines and Geology, scale 1:750,000 (1975).

24. We thank C. Scholz, L. Seeber, A. Nur, and an anonymous reviewer for critical reviews. Scholz pointed out to us literature on changes in fluid pressures in fault zones accompanying a change in normal stress. We thank J. Beavan for providing a copy of the computer program used for calculating changes in stress for planar dislocations. This work supported by grants from the U.S. Geological Survey and the Southern California Earthquake Center. Lamont-Doherty Geological Observatory contribution 5016.

10 August 1992; accepted 23 October 1992

Change in Failure Stress on the Southern San Andreas Fault System Caused by the 1992 Magnitude = 7.4 Landers Earthquake

Ross S. Stein, Geoffrey C. P. King,* Jian Lin*

The 28 June Landers earthquake brought the San Andreas fault significantly closer to failure near San Bernardino, a site that has not sustained a large shock since 1812. Stress also increased on the San Jacinto fault near San Bernardino and on the San Andreas fault southeast of Palm Springs. Unless creep or moderate earthquakes relieve these stress changes, the next great earthquake on the southern San Andreas fault is likely to be advanced by one to two decades. In contrast, stress on the San Andreas north of Los Angeles dropped, potentially delaying the next great earthquake there by 2 to 10 years.

The largest earthquake to strike southern California during the past four decades did not rupture the San Andreas fault, but instead slipped faults within the eastern California shear zone identified previously by geologic (*1*), geodetic (*2*), and mechanical (*3*) methods. Here we show that several smaller shocks that occurred near the Landers event during the preceding 17 years increased stress at the future Landers epicentral site and along much of the eventual rupture path. Similarly, we argue that the Landers earthquake and its aftershocks have changed the stress along the San Andreas fault system.

We used an elastic halfspace boundary

R. S. Stein, U.S. Geological Survey, Mail Stop 977, Menlo Park, CA 94025.
G. C. P. King, Institut de Physique du Globe, Strasbourg 67084, France.
J. Lin, Woods Hole Oceanographic Institution, Woods Hole, MA 02543.

*Visiting Fellows of the Southern California Earthquake Center.

element model to simulate the immediate static response of the crust to earthquakes. The earthquakes were represented in the model by cuts extending from the ground surface to 12.5 km depth using the parameters in Table 1; stress was sampled half way down the fault. To assess the long-term static response after the lower crust has fully relaxed, ~30 to 100 years after the earthquake, we used an elastic plane-stress boundary-element model, in which the seismogenic zone was treated as a 12.5-km-thick plate (*4*).

To gauge the change in proximity to failure of faults in the earth's crust, we calculated the change in the Coulomb failure stress, $\Delta\sigma_f$ [ΔCFF in (*5*)], acting on vertical planes in the crust. Here

$$\Delta\sigma_f = \Delta\tau_s + \mu(\Delta\sigma_n - \Delta P) \qquad (1)$$

where $\Delta\tau_s$ is the static shear stress change (positive in the direction of the regional τ_s) and $\Delta\sigma_n$ is the normal stress change (positive tensile), μ is the static coefficient of friction, and ΔP is the pore pressure change. For plausible fault zone rheologies, Eq. 1 may reduce to $\Delta\tau_s + \mu'(\Delta\sigma_n)$, where $\mu' = \mu(1 - B)$ and B is Skempton's coefficient, which can range between 0 and 1 (*6*). Thus ΔP acts to cancel $\Delta\sigma_n$, and low μ' may be the product of laboratory values of μ (0.75) and high pore fluid pressure ($B \rightarrow 1$). Coulomb failure stress changes were calculated for the 1979 Homestead Valley (*7*), 1984 Morgan Hill (*8*), 1987 Superstition Hills (*9*) and 1989 Loma Prieta (*5, 10*) earthquakes for deduced values of μ' of $0.2 \leq \mu' \leq 0.75$. We examined results for $\mu' = 0.0$, 0.4, and 0.75; the conclusions changed only in detail and so we illustrate the results for $\mu = 0.4$.

The maximum changes in Coulomb failure stress caused by an earthquake occur on planes optimally aligned for failure. The earthquake stress changes plus the regional stress control the orientation of the optimum failure planes. Because the regional stress driving plate motion is larger than the

Table 1. Earthquakes included in the boundary element models.

Earthquake	Date	Moment-magnitude	Moment (dyne-cm)	Length (km)	References
Galway Lake	31 May 1975	5.2	6.3×10^{23}	5	(*25*)
Homestead Valley	15 Mar 1979	5.6	4.2×10^{24}	6	(*7, 26*)
Imperial Valley	15 Oct 1979	6.5	6.0×10^{25}	40	(*17*)
North Palm Springs	7 Aug 1986	6.0	1.1×10^{25}	9	(*27–29*)
Superstition Hills	24 Nov 1987	6.6	1.1×10^{26}	22	(*9, 17*)
Elmore Ranch	24 Nov 1987	6.2	2.5×10^{25}	17	(*9, 17*)
Joshua Tree	23 Apr 1992	6.1	2.2×10^{25}	12	(*27*)
Landers	28 Jun 1992	7.4	1.1×10^{27}	75	(*30–32*)
Big Bear	28 Jun 1992	6.5	5.5×10^{25}	18	(*31*)

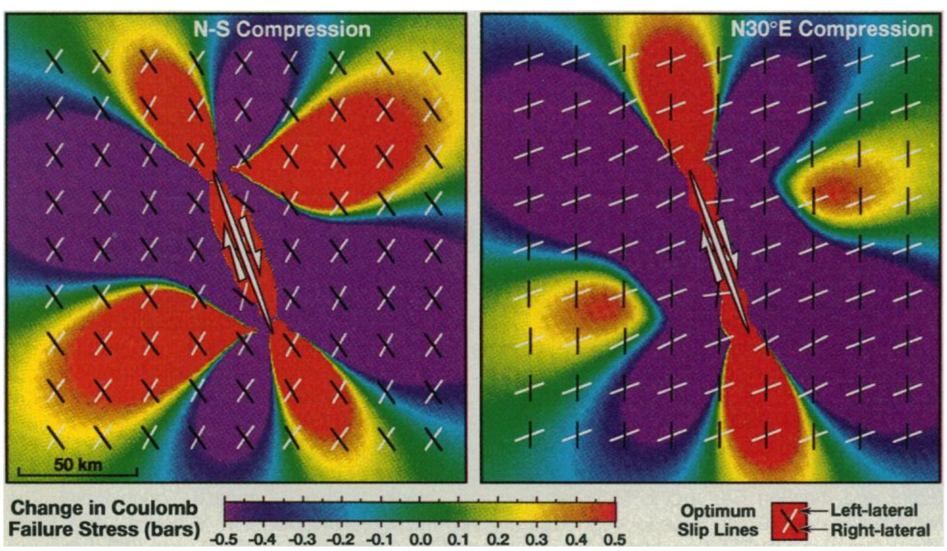

Fig. 1. Example calculations of the maximum Coulomb failure stress change along optimally oriented right-lateral (black) and left-lateral (white) planes, as a function of the regional stress direction. The regional stress magnitude is 100 bars uniaxial compression. The example fault is 70 km long and 12.5 km deep with 5 m of tapered slip and a stress drop of 85 bars. The coefficient of friction ($\mu = 0.4$) controls the angle between the right-lateral and left-lateral planes and the influence of the normal stress on the Coulomb stress. Near the fault, the optimal planes are rotated because the failure stress change is nearly as large as the regional stress.

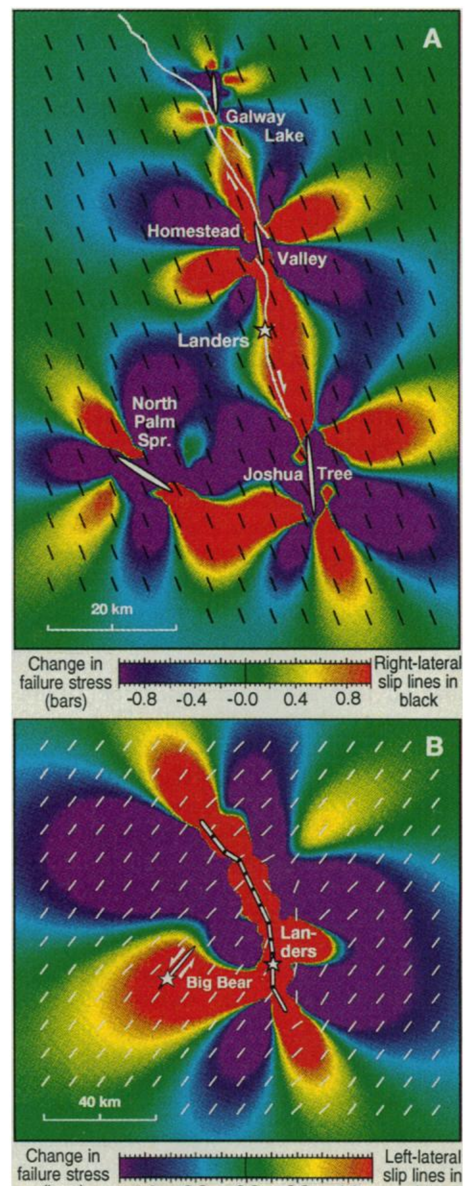

Fig. 2. (**A**) Failure stress changes ($\mu = 0.4$) caused by the four $M_L \geq 5.2$ shocks within 50 km of the Landers earthquake occurring during the 17 years before the right-lateral Landers rupture. The Landers surface rupture tends to lie within the zone of elevated stress change and is favorably oriented for right-lateral failure (black lines). Upper left corner is 34.64°N, 116.84°W; lower left corner is 33.75°N, 116.08°W. (**B**) Failure stress changes ($\mu = 0.4$) preceding the left-lateral Big Bear aftershock of the Landers earthquake. The stress change at the Big Bear epicenter is 3.0 bars and is optimally oriented for left-lateral failure (white lines). The Landers rupture is divided into 11 slip segments from preliminary seismic analyses (*31*) and fault mapping (*32*). From north to south, assigned Landers slip segments are: 1.0, 2.0, 3.0, 4.0, 6.0, 8.0, 5.0, 3.5, 5.0, 3.5, and 0.25 m. Upper left corner is 35.00°N, 117.44°W; lower left corner is 33.66°N, 115.70°W.

stress changes caused by fault slip, the regional stress dominates the orientation of the failure planes except close to the fault (8). Examples of such planes are shown in Fig. 1 for two regional stress directions; a uniaxial compression of 100 bars is used, a value larger than typical earthquake stress drops. In the calculations that follow, we assumed that the regional principal compressive stress was 100 bars and was oriented N7°E, intermediate between the examples of Fig. 1. This is the orientation of principal strain contraction measured from 1934 to 1991 across the Landers and southern San Andreas faults (11). It is also the orientation derived from stress inversion of small shocks along the nearest 50 to 150 km of the San Andreas fault (12). The direction is consistent with the shear strain direction predicted by the motion between the Pacific and North American plates in central California (13), but is discordant with the stress orientation measured in the Cajon Pass well close to the San Andreas fault and 100 km west of the Landers earthquake (14). Our assumptions are valid unless the spatial variability of the true stress field is very high.

Our calculations show that the 1975 Galway Lake, 1979 Homestead Valley, 1986 North Palm Springs, and 1992 Joshua Tree earthquakes (Fig. 2A) (15) increased the Coulomb failure stress by ~1 bar at the future epicenter of the Landers fault. Equally important, the failure stress along most of the future 70-km-long Landers rupture rose by about 1 bar [for comparison, the Landers earthquake stress drop was ~85 bars (16)]. Thus, although we do not know whether the smaller earthquakes were part of a larger process of earthquake preparation, they raised the stress along the future Landers rupture zone and thus advanced the occurrence of the Landers earthquake. The failure stress resolved on the Landers rupture plane is greatest when μ is high, but is still favorable for low μ. The results indicate that all four shocks increased the failure stress at Landers and that the Homestead and Joshua earthquakes contributed the most. Most aftershocks of the 1979 Homestead Valley earthquake occurred in regions where the Coulomb failure stress was predicted to have increased by >0.3 bar (7). In addition, geodetic data suggest that at the site of the future Landers epicenter the fault crept about 10 cm during the 2 years following the Homestead earthquake (7). Thus some parts of the Landers fault were apparently near failure 12 years ago; 2 months before the Landers rupture, the Joshua Tree earthquake further increased the stress.

The same process of stress transfer can be observed with the apparent triggering of the Big Bear earthquake 3 hours 26 minutes after the Landers shock. The Landers rupture is predicted to have increased the proximity to failure at the Big Bear epicenter by 3 bars (Fig. 2B). The stress change predicted at Big Bear is increased for high μ. The rupture plane of the Big Bear shock is optimally aligned for failure, lies in the largest lobe of enhanced Coulomb failure stress resulting from the Landers event, and terminates where the failure stress change became negative in the model. Aftershocks during 25 days after the main shock occurred in regions where the results indicate that the failure stress increased by ≥0.1 bar (Fig. 3). Even when earthquakes within 5 km of the Landers, Big Bear, and Joshua Tree faults are excluded, more than 75% of the remaining aftershocks occur where the stress is predicted to have increased by ≥0.5 bar. In contrast, less than 25% of the aftershocks violate our prediction and occurred where the stress is calculated to have dropped by ≥0.5 bar. Faults predicted to have been loaded by the Landers rupture include the San Jacinto, Camp Rock, Lenwood, Blackwater, Pisgah, and eastern Gar-

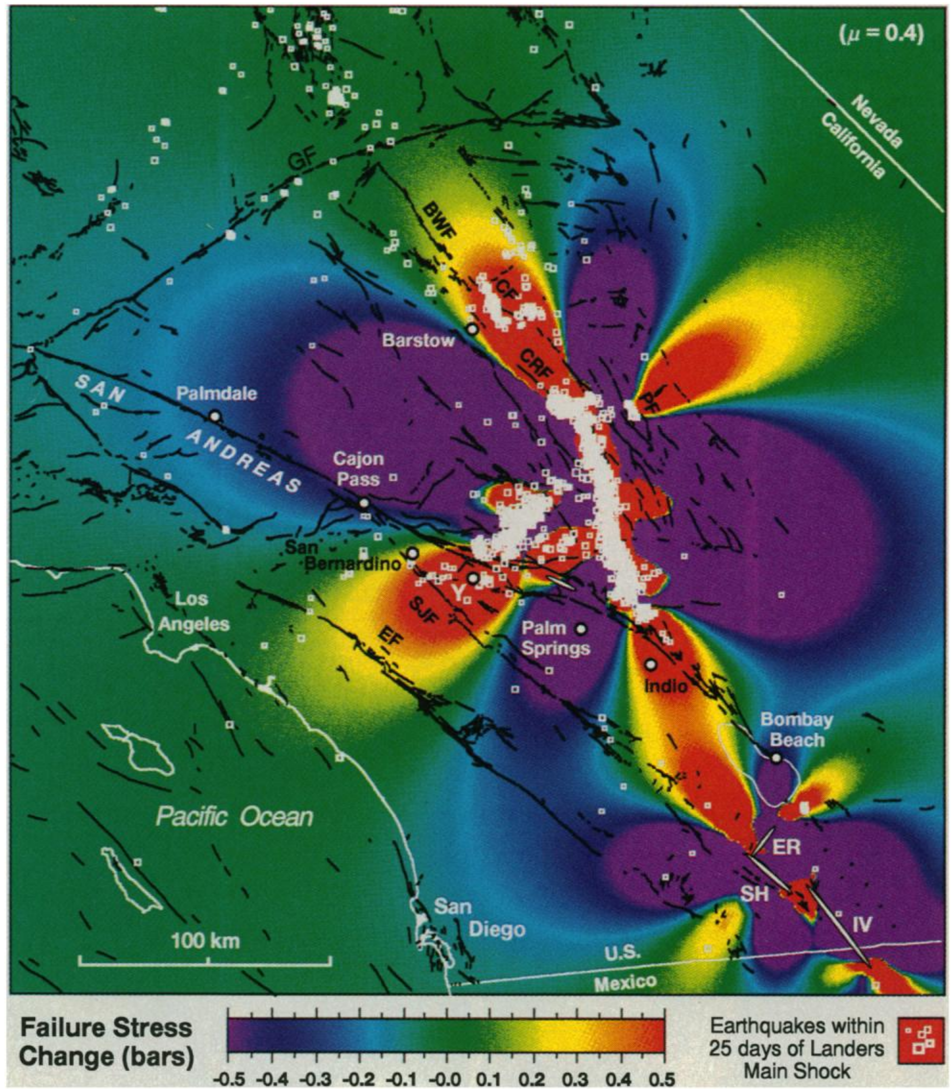

Fig. 3. Coulomb failure stress changes (μ = 0.4) caused by **M** ≥ 6 earthquakes in southeastern California from 1979 to 1992. Quaternary faults are black; the coastline is white. M_L ≥ 1 earthquakes within 25 days of the Landers shock are from the Caltech–U.S. Geological Survey RTP network (root mean square ≤ 0.4 s, ≥7 arrivals). Most Landers aftershocks are found where the predicted failure stress change is positive. Stress changes caused by the 1979 Imperial Valley (IV), 1987 Elmore Ranch (ER), and Superstition Hills (SH) earthquakes are included, but their aftershocks are not shown. Predicted stress has risen along the Coachella Valley segment (Bombay Beach to north of Indio) and the San Bernardino Mountain segment (North of Palm Springs to Cajon Pass). The Mojave segment (Cajon Pass to west edge of map) has been unloaded. Y, Yucaipa. Other faults shown are Elsinore (EF), San Jacinto (SJF), Garlock (GF), Camp Rock (CRF), Pisgah (PF), Lenwood (LF), and Blackwater (BF). Upper left corner is 36.00°N, 119.00°W; lower left corner is 32.50°, 115.00°W.

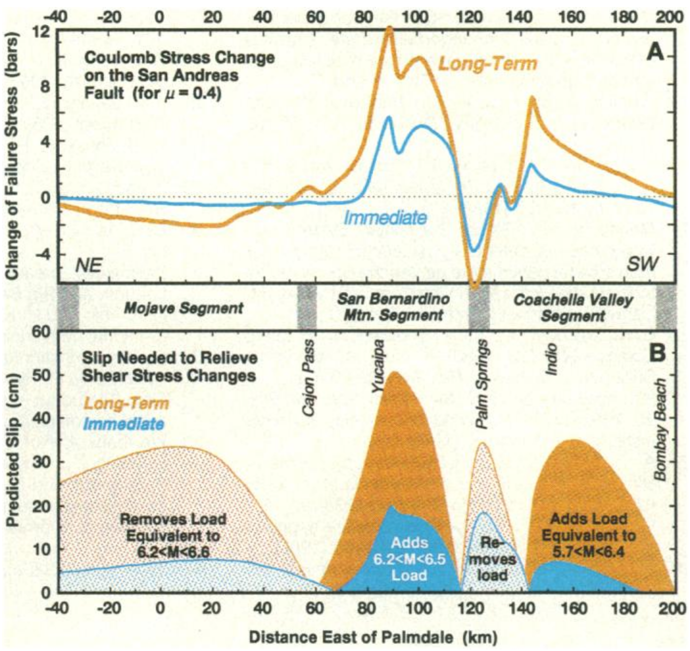

Fig. 4. (**A**) Change in the Coulomb failure stress resolved on the San Andreas fault caused by **M** ≥ 6 earthquakes in southeastern California since 1979. Model fault is vertical and passes between the two branches of the San Andreas fault east of Yucaipa. (**B**) Corresponding slip distribution along the San Andreas fault needed to relieve shear stress imposed by **M** ≥ 6 earthquakes since 1979. Immediate changes are calculated in an elastic halfspace, and so the base of the fault restrains displacement. Long-term changes are calculated in an elastic plate with upper and lower surfaces that are stress-free. Induced right lateral slip (added loads) are solid fields; left lateral slip (removed loads) are stippled.

lock, all of which had Landers aftershocks. An exception occurs near Indio, where the results indicate that the San Andreas fault has been loaded both by the Landers earthquake and, to a lesser extent, by the Imperial Valley, Elmore Ranch, and Superstition Hills events (*17*), but few aftershocks are seen (*18*).

Segment boundaries inferred for the San Andreas fault (*19*) accord roughly to sign changes in the failure stress increments that we conclude were imposed by the Landers event. In Fig. 4A the failure stress change is resolved on the San Andreas fault, rather than on the azimuth of maximum stress change as shown in Figs. 1 to 3. The calculation for Fig. 4 is independent of the magnitude, uniformity, and orientation of the regional stress, and depends only on fault geometry. The failure stress change is positive in the central Coachella Valley segment, negative at the segment boundary north of Palm Springs, and is greatest in the San Bernardino Mountain segment (site of a magnitude M_L = 4.4 aftershock 37 minutes before the Big Bear shock). All of the Mojave segment is negative (Fig. 4A). The stress change calculated on the northern San Jacinto fault southeast of San Bernardino, which is more favorably oriented than the San Andreas fault, is +1 bar. The predicted stress change resolved on the San Andreas fault increases with μ, because tension normal to the fault is enhanced.

The correspondence between seismicity and the Coulomb failure stress changes produced by the Landers and earlier events suggests that regions of predicted increase are candidates for future major events. To predict how the Landers earthquakes have advanced or delayed the next great southern San Andreas earthquake, we let a frictionless San Andreas slip freely to relieve the stress imposed by the Landers and surrounding earthquakes (Fig. 4B). The calculated slip does not depend on the number of segments allowed to slip at once. The immediate response is slip of 20 cm over 30 km of the central San Bernardino segment (equivalent to a magnitude **M** = 6.2 event if it occurred seismically) and 7 cm in the northern Coachella Valley segment (equivalent to **M** = 5.7). Thus on the San Andreas fault slip with a moment equivalent to two moderate events is needed simply to relieve the stresses added by the recent earthquakes. In contrast, a load comparable to an **M** = 6.2 event is removed from the Mojave segment, and an **M** = 6.0 load is removed north of Palm Springs (*20*); thus, these parts of the fault are taken further from failure. After relaxation of the viscous substrate in our idealized plate model, the stress change on the San Andreas and surrounding faults roughly doubles (Fig. 4A, orange curve), as stress is transferred from the base of the fault back to the upper crust. Similarly, the slip required to relieve the stresses also rises (Fig. 4B, orange fields). So far no creep has been measured (*21*), and no moderate earthquakes have occurred on these faults since the Landers event. If these events do not take place, the likelihood of great earthquakes on the San Andreas must rise as well.

Because the southern San Andreas fault is likely late in the earthquake cycle, the long-term probability of a great earthquake on any of its three southern segments was high before the Landers earthquake took place (*19*). The San Bernardino Mountain segment last ruptured in 1812 (*22*); in consideration of its slip rate of 24 ± 3 mm/year (*23*), a slip deficit of ≥4.3 m has since accumulated, which could yield an **M** ≥ 7.5 event. The Coachella Valley segment last ruptured in 1680, has a slip rate of 25 to 30 mm/year, and thus has accumulated a deficit of ≥6 m (**M** ≥ 7.5). Its prehistoric repeat time is ≥235 years (*24*). The Mojave segment last ruptured in 1857, has a slip rate of ~35 mm/year (*23*), and thus has accumulated a deficit of 4.7 m (**M** ≥ 7.7); its repeat time is ~130 years (*22*). The San Bernardino Valley segment of the San Jacinto fault may have last ruptured in 1890; it has a slip rate of 8 ± 3 mm/year (*19*) and thus has a slip deficit of ≥0.8 m (**M** ≥ 6.8).

We estimated the advance and delay times of great earthquakes on the San Andreas by dividing the slip required to relieve the applied stress (Fig. 4B) by the local San Andreas or San Jacinto slip rates. The calculation is independent of the great earthquake repeat times or stress drops, for which there is considerable uncertainty. Our estimate is bounded by the difference between the slip predicted for immediate and long-term periods. We find that the next great San Andreas earthquake along the San Bernardino Mountain segment will strike 8 to 22 years sooner than it would have in the absence of the Landers shock. Similarly, the next great San Andreas earthquake along the Coachella Valley segment is advanced by 2 to 14 years, and the next large earthquake on the San Bernardino Valley segment of the San Jacinto fault is advanced 8 to 56 years. In contrast, we estimate that the next great Mojave shock will be delayed by 2 to 10 years. An earthquake of **M** ≥ 6 on the Mojave segment during the next 2 years would thus falsify our hypothesis.

REFERENCES AND NOTES

1. R. K. Dokka and C. J. Travis, *Geophys. Res. Lett.* 17, 1323 (1990).
2. J. C. Savage, M. Lisowski, W. H. Prescott, *ibid.*, p. 2113.
3. A. Nur, H. Ron, O. Scotti, in *Slow Deformation and Transmission of Stress in the Earth*, S. C. Cohen and P. Vaníček, Eds. (*Geophys. Monogr. 49*, American Geophysical Union, Washington, DC, 1989), p. 31.
4. The halfspace program incorporates the elastic dislocation code of Y. Okada [*Bull. Seismol. Soc. Am.* **82**, 1018 (1992)] into the framework of S. L. Crouch and A. M. Starfield [*Boundary Elements in Solid Mechanics* (Unwin, London, 1983)]. The plane-stress boundary-element program [see R. G. Bilham and G. C. P. King, *J. Geophys. Res.* **94**, 204 (1989); G. C. P. King and M. Ellis, *Nature* **348**, 20 (1990)] runs on Macintosh computers, and is available from King. Poisson's ratio, *v*, is 0.25 and Young's modulus, *E*, is 8.8 × 10^{11} dyne-cm^{-2}.

5. P. A. Reasenberg and R. W. Simpson, *Science* **255**, 1687 (1992).
6. J. R. Rice, in *Fault Mechanics and Transport Properties of Rock*, B. Evans and T.-F. Wong, Eds. (Academic Press, London, 1992), pp. 475.
7. R. S. Stein and M. Lisowski, *J. Geophys. Res.* **88**, 6477 (1983). The moment used for the Homestead Valley earthquake includes postseismic slip, consistent with measured deformation from 1979 to 1981.
8. D. H. Oppenheimer, P. A. Reasenberg, R. W. Simpson, *J. Geophys. Res.* **93**, 9007 (1988).
9. K. W. Hudnut, L. Seeber, J. Pacheco, *Geophys. Res. Lett.* **16**, 199 (1989); S. Larsen, R. Reilinger, H. Neugebauer, W. Strange, *J. Geophys. Res.* **97**, 4885 (1992).
10. R. W. Simpson and P. A. Reasenberg, *U.S. Geol. Surv. Prof. Pap.*, in press.
11. M. Lisowski, J. C. Savage, and W. H. Prescott [*J. Geophys. Res.* **96**, 8369 (1991)] found a principal contractive strain rate of N7 ± 1°E from trilateration surveys conducted since 1979 in the Joshua geodetic network, which includes most of the Landers rupture. J. Sauber, W. Thatcher, and S. C. Solomon [*J. Geophys. Res.* **91**, 12683 (1986)] found that the most compressive principal strain direction measured from 1934 to 1982 across the north half of the Landers rupture was N4 ± 5°E from triangulation surveys.
12. L. M. Jones, *J. Geophys. Res.* **93**, 8869 (1988). The mean of the principal stress directions for the two segments that abut the Landers site, Banning and Indio, is N6 ± 2°E. P. L. Williams, L. R. Sykes, C. Nicholson, and L. Seeber [*Tectonics* **9**, 185 (1990)] found that an average principal stress direction for the adjacent 50-km stretch of the San Andreas fault (San Gregorio Pass and Eastern Transverse Range-I regions) was N8 ± 5°E.
13. C. DeMets, R. G. Gordon, D. F. Argus, S. Stein, *Geophys. J. Int.* **101**, 425 (1990). The Pacific–North American plate motion vector for central California is N36 ± 2°W, which yields a principal compression oriented N9 ± 2°W.
14. M. D. Zoback and J. H. Healy, *J. Geophys. Res.* **97**, 5039 (1992). The Cajon Pass well yields an N57 ± 19°E principal stress direction. If permanent, this stress could not drive local right-lateral slip on the San Andreas fault, and has been interpreted to suggest that the San Andreas is a weak (low μ) fault embedded in a strong (high μ) crust [see M. D. Zoback and A. H. Lachenbruch, *ibid.*, p. 4991]. The stress measured in the well may be influenced by local faults (G. Shamir and M. D. Zoback, *ibid.*, p. 5059) and thus not represent a regional value.
15. All earthquakes in this study except North Palm Springs occurred on near vertical faults with dominant strike slip. We simulated the 30% dip-slip component and 59° dip of the North Palm Springs rupture by including a fault-closing (for example, dike deflation) displacement equal to cos(rake) × cos(dip). This approximation gives accurate stresses at distances greater than one fault length from the source.
16. The mean static shear stress drop calculated from the parameters in Table 1 following H. Kanamori and D. L. Anderson [*Bull. Seismol. Soc. Am.* **65**, 1073 (1975)].
17. C. E. Johnson and D. P. Hill, *U.S. Geol. Surv. Prof. Pap. 1254*, 15 (1982); S. H. Hartzell and T. H. Heaton, *Bull. Seismol. Soc. Am.* **73**, 1553 (1983); T. C. Hanks and C. R. Allen, *ibid.* **79**, 231 (1989); K. Hudnut *et al.*, *ibid.*, p. 282 (1989).
18. Landers aftershocks could be absent in the Coachella Valley because the total stress there is lower or because the strength is higher. We examined the effect of a low modulus Mojave tectonic block embedded in a stiffer crust, consistent with the P_g velocity contours of T. M. Hearn and R. W. Clayton [*Bull. Seismol. Soc. Am.* **76**, 495 (1986)]. The average velocity contrast between the Mojave region (100 by 300 km) with P_g velocity <6.2 km/s and the surrounding medium is 0.45 km/s. We gave the Mojave block a Young's modulus, *E*, of 6.2×10^{11} dyne-cm^{-2} bars. In this plane stress calculation, the Coulomb failure stress increase was halved in the Coachella Valley, but is nearly unchanged elsewhere. Thus it is possible that we overestimated the stress change for the Coachella Valley in Figs. 3 and 4.
19. Working Group on California Earthquake Probabilities, *U.S. Geol. Surv. Open-File Rep. 88-398* (1988).
20. Site of the 1948 **M** = 6.0 Desert Hot Spring earthquake; see L. R. Sykes and L. Seeber, *Geology* **13**, 835 (1985).
21. Monitoring with Global Positioning System networks has not detected postseismic slip greater than several centimeters across the San Andreas fault at Cajon Pass and in the Coachella Valley (M. Lisowski, personal communication).
22. G. C. Jacoby, Jr., P. R. Shepard, K. E. Sieh, *Science* **241**, 196 (1988); K. Sieh, M. Stuiver, D. Brillinger, *J. Geophys. Res.* **94**, 603 (1989).
23. R. J. Weldon II and K. E. Sieh, *Geol. Soc. Am. Bull.* **96**, 793 (1985); R. J. Weldon II, thesis, California Institute of Technology (1986).
24. A. G. Lindh, in *Earthquake Prediction: Present Status*, S. K. Guha and A. M. Patwardhan, Eds. (University of Poona, Pune, India, 1988), p. 189. Repeat times for the Coachella Valley segment are based on K. E. Sieh, *Eos* **67**, 1200 (1986).
25. R. L. Hill and D. J. Beeby, *Geol. Soc. Am. Bull.* **88**, 1378 (1977); A. Lindh, G. Fuis, C. Mantis, *Science* **201**, 56 (1978).
26. N. E. King, D. C. Agnew, F. Wyatt, *Bull. Seismol. Soc. Am.* **78**, 1693 (1988).
27. J. C. Savage, M. Lisowski, W. H. Prescott, *Eos* **73** (Fall Suppl.), 364 (1992).
28. L. M. Jones, K. Hutton, D. A. Given, C. R. Allen, *Bull. Seismol. Soc. Am.* **76**, 1830 (1986).
29. J. Pacheco and J. Nábelek, *ibid.* **78**, 1907 (1988); S. Hartzell, *J. Geophys. Res.* **94**, 7515 (1989).
30. C. J. Ammon, A. A. Velasco, T. Lay, in preparation.
31. Preliminary broad band measurements of the Landers and Big Bear seismic moments are from H. K. Thio and H. Kanamori and from G. Ekström (personal communication).
32. Fault slip function from preliminary fault mapping by D. Ponti, M. Rymer, and K. Lajoie and from K. Sieh, K. Hudnut, C. Rubin, and T. Rockwell (personal communication).
33. We thank A. Nur, R. Weldon II, W. Thatcher, L. Jones, and J. Savage for thoughtful reviews and R. Simpson and R. Harris for stimulating discussion. We are grateful for financial support from the Southern California Earthquake Center.

25 August 1992; accepted 22 October 1992

Accumulation of Suspended Barite at Mesopelagic Depths and Export Production in the Southern Ocean

Frank Dehairs, Willy Baeyens, Leo Goeyens

The relation between the accumulation of barite ($BaSO_4$) microcrystals in suspended matter from the mesopelagic depth region (100 to 600 meters) and the type of production in the euphotic layer (new versus recycled) was studied for different Southern Ocean environments. Considerable subsurface barite accumulated in waters characterized by maintained new production and limited grazing pressure during the growth season. On the other hand, little if any barite accumulated in areas where relatively large amounts of photosynthetically fixed carbon were transferred to the microheterotrophic community and where recycled production became predominant.

In the pelagic oceanic environment, microcrystalline barite (~1 μm) precipitates during the process of organic matter degradation (*1, 2*). This barite accounts for between 50 and 100% of the total Ba in oceanic suspended matter (*1–3*). Although the mechanism of barite formation is unknown, it has been suggested that during degradation of planktonic proteinaceous material sufficient sulfate is produced that barite reaches saturation and barite crystals form (*2*). This seems to be precipitation confined to microenvironments composed of aggregates of biogenic detritus (*1–4*). Supersaturation conditions for barite inside microenvironments can account for the presence of barite in seawater that is undersaturated (*5*). The settling of barite crystals associated with this biogenic detritus to the deep sea and its sediments can explain the observed relation between barite accumulation in the sediments and productivity in overlying surface waters (*6*). Recently, observations of particulate Ba fluxes, as sampled by sediment trap in the intermediate and deep water column, highlight the strong relation between barite and productivity and stress the potential for sedimentary barite fluxes to provide quantitative information on the paleoproductivity of the oceans (*7*). However, part of the detrital aggregates formed in surface waters decompose at mesopelagic depths (*2, 3*). During this process, the carried barite is released as discrete crystals. This release leads to a maximum in the amounts of particulate Ba at depths of 100 to 600 m. Such a maximum is characteristic of large sections of the world ocean, including the Southern Ocean (*1, 2, 8, 9*). Here, we focus on the relation between barite accumulation in mesopelagic waters and the type of production in the euphotic layer of the ocean and compare different Southern Ocean environments.

Analytical Chemistry Department, Vrije Universiteit Brussel, Pleinlaan 2, B-1050 Brussels, Belgium.